Molecular dynamic study on changing pH trends in salt brine evaporation

Yanfang Ma[a,b,c,d], Xin Liu[a,b,e,f], Wanqiu Dong[d], Kanshe Li[d,*], Zhihong Zhang[a,b], Zhiwei Li[a,b,e], Guojian Liu[f], Shaoji Xiang[c,g], Zhenhua Cui[c,g]

[a]Key Laboratory of Comprehensive and Highly Efficient Utilization of Salt Lake Resources, Qinghai Institute of Salt Lakes, Chinese Academy of Sciences, Xining 810008, China, emails: zhangzh@isl.ac.cn (Z. Zhang), mayanfag@isl.ac.cn (Y. Ma) lizw@isl.ac.cn (Z. Li)
[b]Key Laboratory of Salt Lake Resources Chemistry of Qinghai Province, Xining 810008, China
[c]Innovation Academy for Green Manufacture, Chinese Academy of Sciences, Beijing 100190, China, emails: xiangshaoji@163.com (S. Xiang), cuizhenhua@sioc.ac (Z. Cui)
[d]Chemistry and Chemical Engineering College of Xi'an University of Science and Technology, XI'An, Shanxi 710054, China, emails: likanshe@xust.edu.cn (K. Li), 472175377@qq.com (W. Dong)
[e]University of Chinese Academy of Sciences, Beijing 100190, China, email: liuxin192@mails.ucas.ac.cn (X. Liu)
[f]Qinghai Salt Lake Magnesium Co., Ltd., Geermu, Qinghai 81099, China, email: 2298198658@qq.com
[g]Key Laboratory of Organofluorine Chemistry, Shanghai Institute of Organic Chemistry, University of Chinese Academy of Sciences, Chinese Academy of Sciences, Shanghai 200032, China

ABSTRACT

The evaporation and concentration of salt-lake brine is an important preliminary step in the development and utilization of salt-lake resources. The pH value of brine in the Laguocuo salt lake in Tibet has exhibited a gradual decline during the evaporation process, which directly affects lithium resources in salt-lake brine, thereby affecting lithium costs. To study the mechanism of this phenomenon, the evaporation process of salt-lake brine was divided into representative stages and the pH was determined at each stage. Then, an amount of water proportionate to the pH of the water was added; with increasing water content in the system, the pH was observed to increase. The hydration ability of CO_3^{2-} was studied via molecular dynamic simulations and was found to decrease gradually with decreasing water content in the system during evaporation. CO_3^{2-} did not exhibit weak alkaline properties, inducing a decrease in the pH of the system and a shift in the equilibrium of the system from alkaline to acidic.

Keywords: Salt-lake brine; Evaporation; pH; CO_3^{2-} hydration ability; Molecular dynamic

1. Introduction

The Laguocuo salt lake in Tibet is characterized by high lithium and boron contents. It contains trace elements such as lanthanum, cerium, and bromine. The salt lake has a unique water chemistry, which includes both sodium sulfate and weak carbonate. The low Mg/Li ratio is a significant feature of this lake [1]. Additionally, the

pH of the brine decreases gradually after evaporation (pH = 6.48). The lithium content in the brine is ≥30 g/L, and the salt lake supplies good raw materials for the further processing of lithium resources, thus offering incomparable resource advantages over other types of salt lakes. The evaporation and concentration of salt-lake brine is an important preliminary step in the development and utilization of salt-lake resources. The main parameters of the evaporation process(pH, Mg/Li, etc.) provide an important basis for the separation and extraction of lithium [2,3].

* Corresponding authors.

Previous research on salt-lake brine has shown that the concentrated evaporation (continuous evaporation) of salt-lake brine is accompanied by constant changes in the pH of the system. Such changes can be categorized into two types: (1) the pH value may increase [4,5], that is, the system becomes alkaline and (2) the pH value decreases [6–10], that is, the system becomes acidic. Many studies have reported changes in the pH of the system during evaporation [11,12]; however, an in-depth analysis of the pH-change mechanism has not been conducted so far.

The result of the movement of the equilibrium of the system toward a more acidic or alkaline state is reflected by the pH. According to the electric neutrality principle, strong acid ions (Cl^-, SO_4^{2-}, etc.) and strong alkali ions (K^+, Na^+, etc.) in the system can be mixed with salt, a neutral component, without affecting the pH of the system. The water content in the system gradually decreases during evaporation. The role of relatively weak alkaline ions is gradually manifested. The hydrolysis ability of such weak alkaline ions is the main cause of changes in the pH, gradually increasing the pH of the system. In this study, relevant experiments for verification and molecular dynamic (MD) simulations were conducted to explore the regulation of pH variations and understand the cause of pH changes in salt-lake brine. This study can facilitate a deeper understanding of the control of evaporation, thus enabling an improved prediction of the brine evaporation process. Further, the findings of this study can provide a theoretical basis for enriching salt-lake brine and extracting lithium resources.

2. Experimental and computational section

2.1. Determination and analysis of pH changes based on the salt-lake brine concentration

So far, variations in the pH in the Laguocuo salt lake in Tibet during evaporation have been reported. In this study, the pH and density of representative samples collected during the brine evaporation process under isothermal conditions were investigated using a METTLER's Inlab Max Pro-ISM composite-electrode acidity meter.

CO_3^{2-} determination method: CO_3^{2-} was calculated using Eq. (1):

$$CO_3^{2-}\ (mg/L) = \frac{2 \times V_1 \times 60.01 \times M}{V_s} \times 1,000 \tag{1}$$

where M is the concentration of the titrated HCl solution, V_1 is the amount of hydrochloric acid consumed, and V_s is the volume of the sample containing the original brine.

The Laguocuo salt lake is a weak carbonate–type salt lake. It is alkaline based on its initial pH, which gradually decreases during evaporation, becoming acidic.

3. Results and discussion

3.1. pH during the brine evaporation process at the Laguocuo salt lake

The pH and related parameters of the system under isothermal conditions were measured. Based on the five-element phase diagram of Na^+, K^+//Cl^-, SO_4^{2-}, and CO_3^{2-}–H_2O and the crystallization process of brine during evaporation under isothermal conditions, the evaporation process was divided into five stages: unsaturated, thenardite, sodium chloride, potassium thenardite, and potassium chloride stages. The pH of the representative samples obtained at each stage was measured. The pH-change curve representing the evaporation and concentration of brine is shown in Fig. 1, and the corresponding values are detailed in Table 1. The results show that when evaporation occurs, the pH of the brine decreases, becoming acidic.

3.2. Discussion on changes in pH during evaporation

During evaporation, the pH of the brine in the Laguocuo salt lake decreases; this is inconsistent with the theoretical analysis of pH. Therefore, brine comprising Na^+, K^+//Cl^-, SO_4^{2-}, and CO_3^{2-}–H_2O is studied during evaporation. It is necessary to study the regulation of pH variations and the corresponding mechanism. In this system, CO_3^{2-} was instrumental in inducing changes in the pH. The CO_3^{2-} concentrations and pH values in the brine during evaporation are shown in Table 2.

After adding appropriate amounts of deionised water to the five groups of representative brine samples shown in Table 2, the pH of each sample was measured under isothermal conditions. Water was added to 20 g of brine; the corresponding results are shown in Table 3.

The results in Table 3 and Fig. 2 show that after adding water to the brine, the pH increases. The pH value of samples 1#, 2#, 3#, 4#, and 5# varies with the water content as follows: ΔX (ΔX is just the change in value pH of start to end) is 0.18, 0.41, 1.21, 1.89, and 2.74, respectively. Owing to the low total salt content in sample 1#, the pH value shows only a slight change. Alternatively, in sample #5, the maximum change in the pH is observed, possibly related to the binding abilities of CO_3^{2-} and H in the system.

3.3. MD simulations

All Al-atom MD simulations were conducted using the GROMOS54a7 force field [13] created by the automated topology builder [14] and using the Gromacs-4.6.7 software package [15]. One-nanosecond-long NVT and NPT relaxation runs were performed before the production simulation. The time step was 2-fs long, and the total run time for the equilibrium MD simulations was 10 ns. We used the relaxed system as the starting configuration. As it is prior to system relaxation MD, energy minimization was conducted using a composite protocol of steepest descent using termination gradients of 100 kJ/mol nm. A Nosé–Hoover thermostat [16] was used to maintain the equilibrium temperature at 291 K, and periodic boundary conditions were imposed on all three dimensions. The particle Mesh–Ewald method [17,18] was employed to compute long-range electrostatics within a relative tolerance of 1×10^{-6}. A 1.2 nm cut-off distance was applied to real-space Ewald interactions, and the same value was used for van der Waals interactions. The linear constraint solver algorithm [19] was used to constrain the bond lengths of hydrogen atoms. A leap-frog algorithm [20] was used with a 2-fs time step.
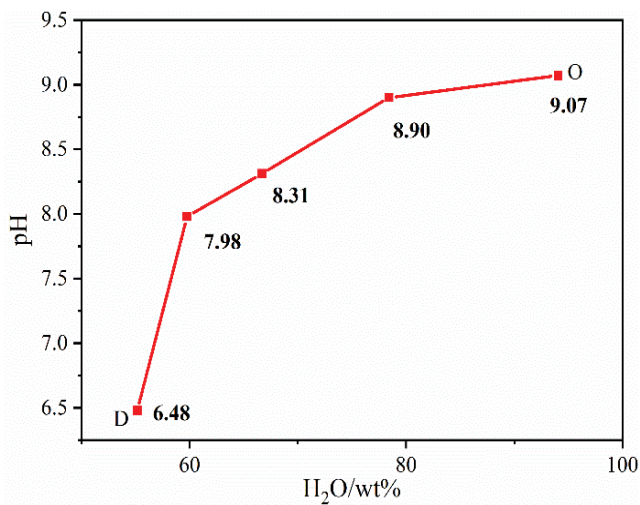
Fig. 1. pH changes during salt-lake brine evaporation under isothermal conditions (O: origin and D: destination).
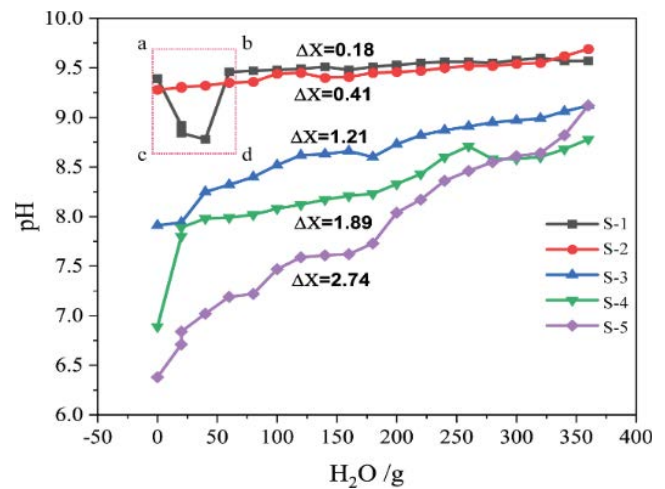

Fig. 2. Changing trend of the pH and water content in the system (S-1: system 1; S-2: system 2; S-3: system 3; S-4: system 4; and S-5: system 5).

Table 1
pH and other parameters during evaporation under isothermal conditions

Samples	1#	2#	3#	4#	5#
Density/g cm^{-3}	1.0519	1.0724	1.1738	1.2770	1.2999
pH	9.07	8.90	8.31	7.98	6.48
H_2O/wt.%	94.06	78.42	66.66	59.75	55.14
Remarks	Unsaturated stage	Thenardite stage	Sodium chloride stage	Potassium thenardite stage	Potassium chloride stage

Table 2
Concentration of CO_3^{2-} and pH

Samples	1#	2#	3#	4#	5#
CO_3^{2-}/mol L^{-1}	0.27	0.52	0.72	0.55	0.46
H_2O/mol L^{-1}	57.79	55.61	51.61	50.24	40.44
Sum of ions/mol L^{-1}	5.01	7.80	17.76	27.54	39.29
pH	9.39	9.28	7.91	6.89	6.38
Remarks	Unsaturated	Mirabilite	Sodium chloride	Arcanite	Potassium chloride

Cube boxes were created with sizes of 5.667, 5.860, 6.386, 6.824, and 6.937 nm. The simulation temperature and pressure were 298 K and 1 bar, respectively.

The process was simulated using the five systems shown in Table 2. The absolute value of the van der Waals force between two ions is very small compared to the electrostatic force; therefore, it can be neglected. The interaction force between two ions mainly originates from the electrostatic force. The absolute value of the electrostatic force first decreases and subsequently increases. The strength of the electrostatic interaction increases with increasing absolute value of the force, implying that the electrostatic interaction between CO_3^{2-} and H is relatively weak under neutral conditions than under acidic or alkaline conditions.

The results in Table 3 show that after adding water to the brine, the pH increases, possibly related to the binding abilities of CO_3^{2-} and H$^+$ in the system.

Figs. 3 and 4 show that the diffusion coefficients of CO_3^{2-} and H first decrease and then increase with decreasing pH, thus proving that CO_3^{2-} and H move faster in acidic or alkaline environments and slower in neutral environments.

Diffusion coefficient is an important index for measuring the diffusion ability of particles. It can be changed by the mean azimuth of the particle (mean square displacement, MSD) [21–23].

The self-diffusion coefficient (*D*) can be calculated using the Einstein–Smoluchowski function [24,25]:

Table 3
Relation between water content in the system and pH

Salt-lake brine/g	H$_2$O/g	pH				
		1#	2#	3#	4#	5#
20	0	9.39	9.28	7.91	6.89	6.38
20	2	8.92	9.30	7.94	7.80	6.71
20	4	8.84	9.31	7.94	7.89	6.84
20	6	8.78	9.32	8.25	7.98	7.02
20	8	9.46	9.35	8.32	7.99	7.19
20	10	9.47	9.36	8.40	8.02	7.22
20	12	9.48	9.44	8.52	8.08	7.47
20	14	9.49	9.45	8.62	8.12	7.59
20	16	9.51	9.40	8.63	8.17	7.61
20	18	9.48	9.41	8.66	8.21	7.62
20	20	9.51	9.45	8.60	8.23	7.73
20	30	9.53	9.46	8.73	8.33	8.04
20	40	9.55	9.47	8.82	8.43	8.17
20	50	9.56	9.50	8.87	8.60	8.36
20	60	9.56	9.52	8.91	8.71	8.46
20	70	9.55	9.52	8.95	8.58	8.55
20	80	9.58	9.54	8.97	8.58	8.61
20	90	9.60	9.55	8.99	8.60	8.64
20	140	9.57	9.62	9.06	8.68	8.82
20	250	9.57	9.69	9.12	8.78	9.12
ΔX		0.18	0.41	1.21	1.89	2.74

Fig. 4. pH and van der Waals force.

Fig. 5. pH and hydrogen-ion diffusion coefficient.

Fig. 3. pH and electrostatic forces.

$$D = \frac{1}{2dt}\left\langle [r(t)]^2 \right\rangle \qquad (2)$$

where D is the self-diffusion coefficient, $r(t)$ is the MSD, and dt is the integration step.

Calculate the value of the obtained H$^+$ and CO$_3^{2-}$, Figs. 5 and 6 show that the diffusion coefficient of hydrogen changed considerably. At pH = 7.5–8.5, the diffusion

Fig. 6. Carbonate concentration and carbonate diffusion coefficient.

coefficient of hydrogen decreased but it decreased gradually with decreasing diffusion coefficient of CO_3^{2-}.

The radial distribution function is an important parameter for describing the molecular architecture [26,27]. The compatibility of the brines improves with increasing value of the radial distribution function $g(r)$. Figs. 7 and 8 show the radial distribution functions of CO_3^{2-} and H in the five studied systems. The results show that the system has a close-range ordered and long-range disordered conformation. Few peaks with different heights and sharpness are observed. The peak intensity decreases rapidly with increasing distance and tends to be evenly distributed at long distances, that is, $g(r) = 1$. From Figs. 7 and 8, the radial distribution functions of CO_3^{2-} and H differ considerably. The CO_3^{2-}–H_2O bond is longer than the H^+–H_2O bond, and the degrees of order and stability are enhanced when the water content decreases. The interaction between CO_3^{2-} and H develops in a more alienated direction.

With increasing total ion concentration and decreasing water content in the simulated system, the first peak of the radial distribution of CO_3^{2-}–H_2O in S-1–S-5 appears at 0.17 Å. The peak value decreases from 1.93 to 0.33 with increasing total ion concentration. In S-1–S-4 system, the second peak of CO_3^{2-}–H_2O appears at 0.27 Å and the peak value decreases from 1.47 to 0.35 with increasing total ion concentration. CO_3^{2-} shows a strong hydration

capacity. In the solution, relatively stable ion pairs or ion clusters are formed with H. However, with an increase in the total ion concentration, the hydration ability of CO_3^{2-} decreases gradually. This explains why the pH of the system decreases as the evaporation of salt-lake brine proceeds.

S-1 showed peak fluctuations at 0.22 and 0.29 Å (Fig. 8), Corresponds exactly to the ΔX value of 1# should equal to 9.39–8.78 = 0.61 (Table 3). Furthermore, the pH (in the box a-b-c-d in Fig. 2) first decreases and then increases. This shows that the pH is related to the active degree of H in the system. H^+ exhibits strong hydration ability at salt-lake brine:H_2O ratios of 10:1–10:3. The hydration capacity of H^+ decreases at the salt-lake brine:H_2O ratio of >10:4. Therefore, the PH value at this stage first decreases and then increases.

Figs. 9 and 10 show the MSDs of the CO_3^{2-} and H atoms in the five studied systems that were simulated when the water content was reduced. These figures show that the CO_3^{2-} and H fluctuations in acidic or alkaline environments are greater than those in neutral environments. This indicates that the forces of CO_3^{2-} and H under acidic and alkaline conditions are stronger than those under neutral conditions during the simulation process and the forces in alkaline environments are greater than those in acidic environments.
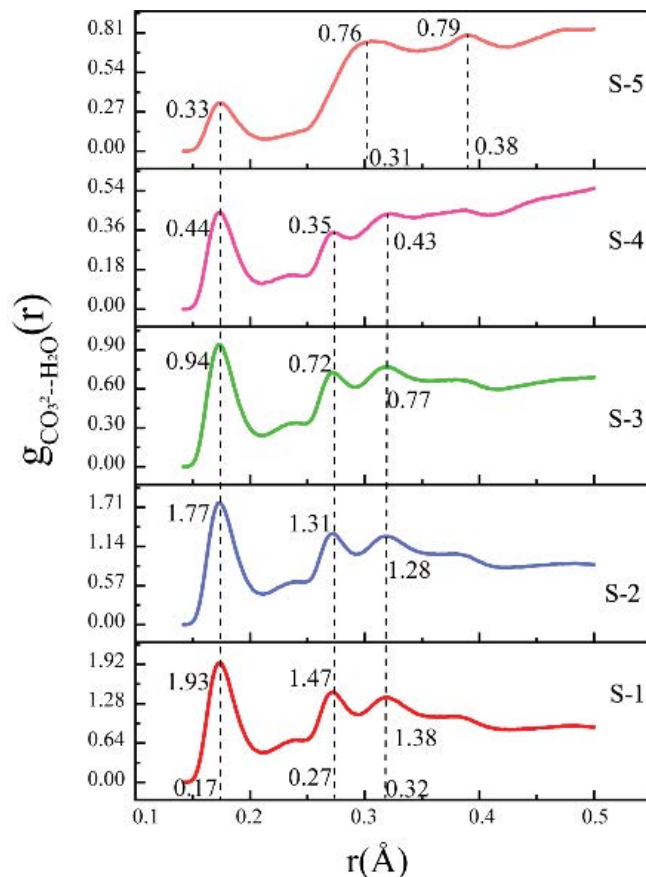

Fig. 7. CO_3^{2-}–H_2O radial distribution function (S-1: system 1; S-2: system 2; S-3: system 3; S-4: system 4; S-5: system 5).
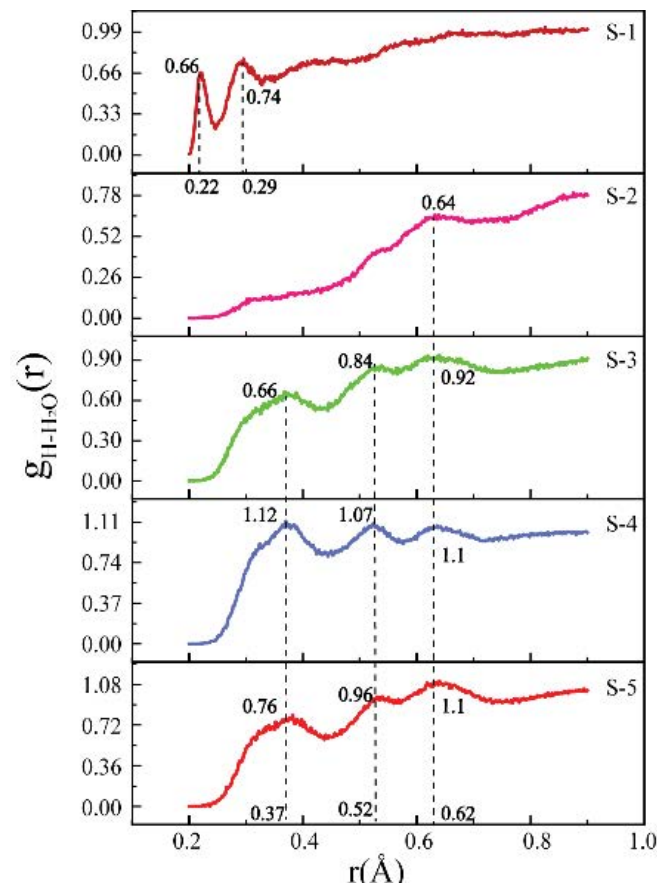
Fig. 8. H^+–H_2O radial distribution function (S-1: system 1; S-2: system 2; S-3: system 3; S-4: system 4; S-5: system 5).
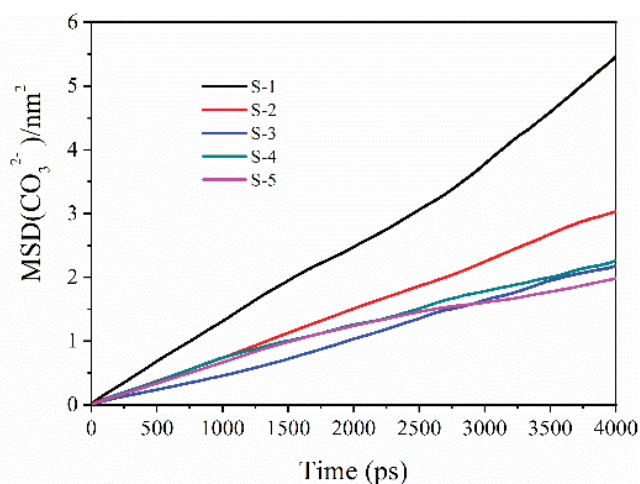
Fig. 9. CO_3^{2-} mean square displacement (S-1: system 1; S-2: system 2; S-3: system 3; S-4: system 4; S-5: system 5).
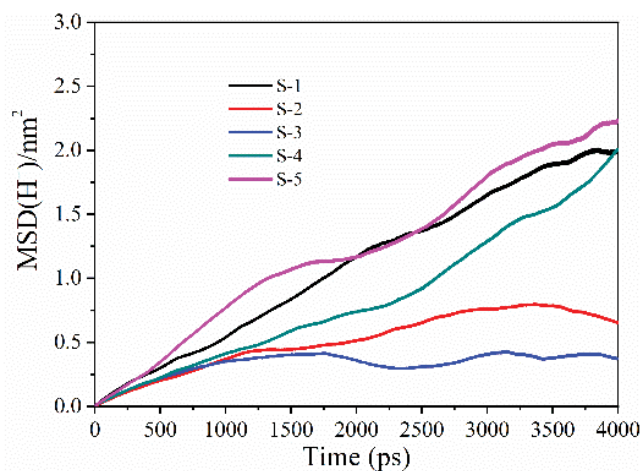
Fig. 10. H mean square displacement (S-1: system 1; S-2: system 2; S-3: system 3; S-4: system 4; S-5: system 5).
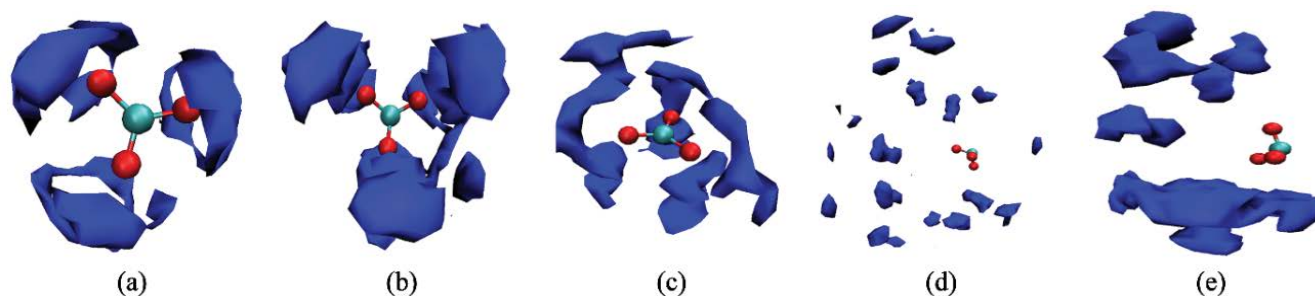

Fig. 11. Spatial distribution function of water around CO_3^{2-} (Blue represents the probability of water appearing in the CO_3^{2-} space).

The spatial distribution of ionized water around CO_3^{2-} was analyzed, as shown in Fig. 11.

S-1–S-5 show that water is present around the oxygen atoms of CO_3^{2-}; this is strongly associated with the formation of hydrogen bonds between water and oxygen atoms. The distance between the water molecules around CO_3^{2-} increases from as the system progresses from 1 to 5. A shell structure is absent in S-4 and S-5, and a strong water shell is observed only in S-1–S-3. The results show that in S-4 and S-5, water is not close to CO_3^{2-}; therefore, it gradually loses its weak alkalinity.

4. Conclusion

The type and intensity of the interactions between CO_3^{2-} and H were investigated via MD simulations, and the microscopic causes of pH changes in the system were explained. The pH changes in carbonated salt-lake brine—obtained from the Laguocuo salt lake—were studied. The experimental results show that the pH value gradually decreases with decreasing water content in the system. The shift from alkaline to acidic is directly related to the hydration ability of the weakly alkaline CO_3^{2-} species in the system. This result was verified and explained via MD simulations. With the water content gradually decreasing in the system, the hydration ability

of CO_3^{2-} showed a downward trend. Thus, its weak alkalinity was reduced further, inducing changes in the pH of the system, thereby making the system increasingly acidic.

Symbols

M	—	Concentration of the titrated HCl solution
V_1	—	Amount of hydrochloric acid consumed
V_s	—	Volume of the sample containing the original brine
D	—	Self-diffusion coefficient
$r(t)$	—	MSD
dt	—	Integration step

References

[1] T. Dong, H.B. Tan, W.J. Zhang, Y.F. Zhang, The geochemical distribution of lithium in salt lakes in Tibet, J. Hohai Univ. (Nat. Sci.), 43 (2015) 230–235.
[2] C. Grosjean, P.H. Miranda, M. Perrin, P. Poggi, Assessment of world lithium resources and consequences of their geographic

distribution on the expected development of the electric vehicle industry, Renewable Sustainable Energy Rev., 16 (2012) 1735–1744.

[3] A.H. Ratner, M.B. Geilikman, S.V. Aleksandrovski, F. Jiang, Thermodynamic calculation on metallic thermoreduction during preparation of aluminum-rare master alloys, Trans. Nonferrous Met. Soc. China, 11 (2001) 18–21.

[4] Z.M. Wu, X.M. Cui, M.P. Zheng, Study on the change of pH value in the process of Salt Lake Brine evaporation and concentration, Chin. J. Inorg. Chem., 28 (2012) 297–300.

[5] Z. Yan, X.P. Yu, X.Y. Wang, MoS_2 nanosheets supported gold nanoparticles for electrochemical nitrogen fifixation at various pH value, Electrochim. Acta, 317 (2019) 34–41.

[6] S. Elwira, G. Michał, The diatom-inferred pH reconstructions for a naturally neutralized pit lake in south-west Poland using the mining and the combined pH training sets, Sci. Total Environ., 605–606 (2017) 75–87.

[7] W.G. Hou, B.B. Hou, S.M. Yang, W.P. Han, S.B. Sun, Determination of sodium content in industrial potassium hydroxide by flame photometer method and atomic absorption method, J. Salt Sci. Chem. Ind., 47 (2018) 27–29.

[8] P. Temporetti, G. Beamud, D. Nichela, G. Baffico, F. Pedrozo, The effect of pH on phosphorus sorbed from sediments in a river with a natural pH gradient, Chemosphere, 228 (2019) 287–299.

[9] B. Wang, Y. Qin, J. Shen, G. Wang, Q. Zhang, M. Liu, Experimental study on water sensitivity and salt sensitivity of lignite reservoir under different pH, J. Pet. Sci. Eng., 172 (2019) 1202–1210.

[10] X.M. Cui, Y.P. Dong, X.Y. Nai, H.T. Feng, J. Li, W. Li, Study on the special crystallization behavior of boron in the evaporation process of oil field brine, Chin. J. Inorg. Chem., 25 (2009) 1434–1441.

[11] P.S. Song, Y. Yao, Thermodynamics and phase diagram of the salt lake brine system at 298.15 K – V. Model for the system Li^+, Na^+, K^+, Mg^{2+}/Cl^-, SO_2^{4-}-H_2O and its applications, Calphad – Computer Coupling of Phase Diagrams and Thermochemistry, 27 (2003) 343–352.

[12] L.Z. Bu, Z. Nie, P.S. Song, Computer simulation of isothermal evaporation process of sodium sulfate subtype lithium-rich brine at 25°C, Acta Sin., 84 (2010) 1708–1710.

[13] N. Schmid, A.P. Eichenberger, A. Choutko, Definition and testing of the GROMOS force-field versions 54A7 and 54B7, Eur. Biophys. J., 40 (2011) 843–856.

[14] A.K. Malde, L. Zuo, M. Breeze, M. Stroet, D. Poger, P.C. Nair, C. Oostenbrink, A.E. Mark, An automated force field topology builder (ATB) and repository: version 1.0, J. Chem. Theory Comput., 7(2011) 4026–4037.

[15] B. Hess, C. Kutzner, D. van der Spoel, E. Lindahl, GROMACS 4: algorithms for highly efficient, load-balanced, and scalable molecular simulation, J. Chem. Theory Comput., 4 (2008) 435–447.

[16] H.J.C. Berendsen, J.P.M. Postma, W.F. van Gunsteren, A. DiNola, J.R. Haak, Molecular dynamics with coupling to an external bath, J. Chem. Phys., 81 (1984) 36–84.

[17] U. Essmann, L. Perera, M.L. Berkowitz, A smooth particle mesh Ewald method, J. Chem. Phys., 103 (1995) 8577–8593.

[18] L.G. Astrakas, C. Gousias, M. Tzaphlidou, Structural destabilization of chignolin under the influence of oscillating electric fields, J. Appl. Phys., 111 (2012) 74–102.

[19] B. Hess, H. Bekker, H.J.C. Berendsen, J.G.E.M. Fraaije, LINCS: a linear constraint solver for molecular simulations, J. Comput. Chem., 18 (1997) 1463–1472.

[20] W.F. Van Gunsteren, H.J.C. Berendsen, A leap-frog algorithm for stochastic dynamics, Mol. Simul., 1 (1988) 173–185.

[21] C. Caleman, D. van der Spoel, Evaporation from water clusters containing singly charged ions, Phys. Chem. Chem. Phys., 9 (2007) 5105–5111.

[22] J. Zhang, M.K. Borg, K. Sefiane, J.M. Reese, Wetting and evaporation of salt-water nanodroplets: a molecular dynamics investigation, Phys. Rev., 92 (2015) 52–54.

[23] J. Zhang, M.K. Borg, K. Ritos, J.M. Reese, Electrowetting controls the deposit patterns of evaporated salt water nanodroplets, Langmuir, 32 (2016) 1542–1549.

[24] J. Wang, R.M. Wolf, J.W. Caldwell, P.A. Kollman, D.A. Case, Development and testing of a general amber force field, J. Comput. Chem., 25 (2001) 1157–1174.

[25] K.J. Tielrooij, S.T. van der Post, J. Hunger, M. Bonn, H.J. Bakker, Anisotropic water reorientation around ions, J. Phys. Chem. B, 115 (2011) 12638–12647.

[26] Q.G. Li, C.Z. Xin, W.Z. Zhang, W. Zheng, L. Liu, S. Wu, Protection mechanism of antioxidant for thermo-oxidative ageing of natural rubber with combination of experimental and molecular dynamics simulation, Polym. Mater. Sci. Eng., 34 (2018) 106–111.

[27] Y.S. Li, X.B. Zhang, T.H. Huang, F.Q. Meng, Y.L. Xie, Molecular dynamics simulation of SiO_2/XLPE in humid environment, J. Mol. Sci., 35 (2019) 209–221.